Lowland Technology International 2015; 17 (3): 157-166
International Association of Lowland Technology (IALT): ISSN 1344-9656

Research Paper

3D FEM investigation on bending failure mechanism of column inclusion under embankment load

S. Shrestha [1], J.-C. Chai [2], D.T. Bergado [3], T. Hino [4] and Y. Kamo [5]

ARTICLE INFORMATION

Article history:

Received: 03 January, 2015
Received in revised form: 17 October, 2015
Accepted: 03 November, 2015
Published: December, 2015

Keywords:

3D FEA
Tensile failure
Embankment
DCM column
Centrifuge

ABSTRACT

Bending failure mechanism of column inclusions in soft clay deposit under embankment loading has been investigated by three dimensional (3D) finite element analyses. Firstly the effectiveness of the numerical procedure has been verified by comparing the simulated and the measured results of a centrifuge model test reported in the literature in terms of lateral displacement, settlement, and the bending moment in the column. Then the effects of the size of the column improved area from the toe toward the center of the embankment, stiffness of the column, the length of the column on the maximum bending moment in the column have been investigated numerically. The numerical results indicate that increase the size of the improved area, reduced the bending moment in the upper part (near ground surface) of the column; increase the stiffness of the column increased the maximum bending moment; and the maximum bending moment occurred at the end of the column in the case of an end bearing column, and in the upper part of the column for a floating column. The numerical results also indicate that when the whole area under the embankment is improved by end bearing columns with an area improvement ratio of 28 % and tensile strength of the column of 100 kN/m^2, the embankment load can be applied with a factor of safety of about 2 for bending failure of the columns is about 13 times of the initial undrained shear strength of the soft deposit.

1. Introduction

Deep cement mixing (DCM) formed columns have been widely used to improve soft clayey deposit for highway embankment constructions. To reduce construction cost and minimize the possible effect on the ground water, improvement of the soft clayey deposit by floating DCM columns has been applied to several field projects (Shen et al. 2001; Chai et al. 2009; Chai and Carter 2011; Hino et al. 2012). Numerous researches have been already carried out to study the failure mode of embankments on DCM columns improved deposit either by numerical modelling or physical modelling and case histories of field performance (Broms 2004; Kitazume and Maruyama 2007). While, current design methods consider the shear failure of DCM columns for internal stability as shown in Fig. 1, but this kind of failure mechanism has not been verified experimentally and numerically.

[1] Corresponding author, PhD Candidate, Saga University, Saga, JAPAN, shresthasailesh@gmail.com
[2] Professor, Department of Civil Engineering and Architecture, Saga University, Saga, JAPAN, chai@cc.saga-u.ac.jp
[3] Distinguished Adjunct Professor, School of Engineering and Technology, Asian Institute of Technology, THAILAND, dbergado@gmail.com
[4] Professor, Institute of Lowland and Marine Research (ILMR), Saga University, Saga, JAPAN, hino@ilt.saga-u.ac.jp
[5] JIP Techno Science Corporation, Tokyo, JAPAN, yukihiko_kamo@cm.jip-ts.co.jp
Note: Discussion on this paper is open until June 2016.

Based on the results of a series of centrifuge model tests for embankment on column improved model ground, Kitazume and Maruyama (2007) found that bending failure occurred instead of shear failure (Fig. 2a). Yapage et al. (2013a; 2013b) analyzed geosynthetic reinforced column supported (GRCS) embankments using two dimensional (2D) finite element analysis (FEA) and found punching shear failure around column heads, overturning failure and bending failure of DCM columns. Zhang et al. (2014) used 3D FEA to investigate the failure modes of DCM column supported embankments on soft soils and found out bending deformation of the columns with one and two plastic hinges. Similarly, Shrestha et al. (2015) conducted 3D FEA simulating centrifuge model tests of embankment on column improved clayey soil, and found bending failure occurred first in the column.

However, it is still not clear about the conditions under which the bending failure of columns will occur. In this paper, one of the centrifuge model tests reported by Kitazume and Maruyama (2007), Case 3 has been simulated by 3D FEA first to verify the numerical procedure by comparing the measured and simulated results in terms of lateral displacements and bending moments in the model columns. With verified numerical procedure, further numerical investigations have been conducted on the effects of (a) improved area; (b) height of the embankment; (c) length of columns (floating versus end bearing); and (d) stiffness of the column to the bending moment in the columns. The numerical modeling procedure is presented first, followed by the numerical results and comparison with the measured results of the centrifuge model test. Then the factors affecting the bending moment in the columns and bending failure mechanism are discussed using numerical results.

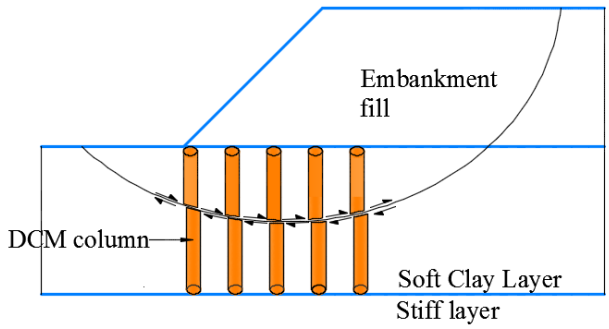

Fig. 1. Shear failure.

2. Finite element modelling

2.1 Description of the centrifuge model tests

The centrifuge tests reported by Kitazume and Maruyama (2007) used a box with dimensions of 0.7 m in length, 0.2 m in width and 0.6 m in depth. The height of the embankment was 0.2 m and the subsoil consisted of 0.2 m thick soft clay layer underlain by a 0.2 m thick dense sand layer (Fig. 3). The tests were conducted under 50 g, and for a prototype model, it would be an embankment with height of 10 m on a 10 m thick soft clay layer. The engineering properties of the embankment, clay layer, and sand layer are listed in Table 1. Referring the data provided by Kitazume and Maruyama (2006), two types of model columns, an acrylic pipe and a soil-cement column, were used in the centrifuge model tests, and their dimensions and Young's moduli are listed in Table 2.

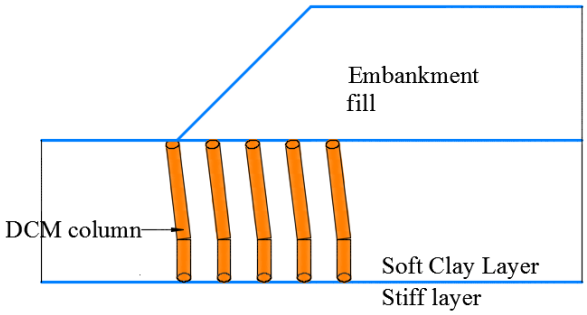

(a) Bending failure

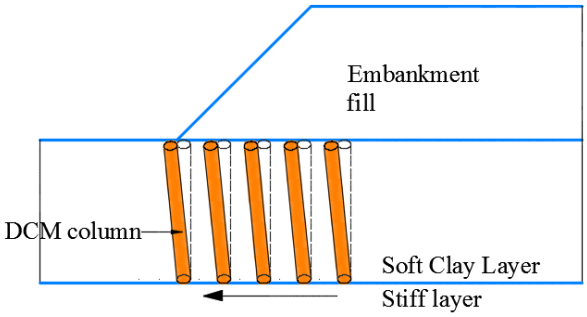

(b) Collapse failure (Column with high strength and stiffness)

Fig. 2. Failure modes of DCM columns (Kitazume and Maruyama, 2007).

The annular acrylic pipe was filled with a steel rod and silicon to make the self-weight of the pipe close to the model ground. Strain gauges were installed on the outer surface of the pipe to measure the bending moment distribution (Kitazume and Maruyama 2006). While with soil-cement column, the bending moment was not able to be measured. For the centrifuge test Case 3, the model ground was improved by five rows of acrylic pipes fully penetrated into the soft clay layer under the toe of the embankment. The pipes were arranged in a square pattern with a spacing of 33 mm. Other centrifuge test Cases 2 and 4, the model ground were improved by acrylic pipes but with three and seven rows. In the centrifuge test Case 7, the soil-cement columns were used but with same

number of rows as in Case 3. For all the cases, the area improvement ratio was 0.28.

2.2 Simulation procedure

In simulating the centrifuge model test, the geometry of the model, the physical and mechanical properties of the model ground and loading procedure have been modelled the same as the actual ones. The gravity force is 50 times of the earth gravity (n = 50), and in term of consolidation time, suppose the centrifuge time is t_c, which correspond to a time of $n^2 \cdot t_c$ for a full scale prototype case.

2.3 3D modelling of the columns

In 3D FEA, the column was modeled as a solid elements with a square cross-sectional area for the ease of mesh generation (Chai et al. 2015). For columns used in the model test Case 3, the value of the second moment of area I, a value of each column as 6.37×10^{-9} m^4 can be estimated. Under the condition of equal EI (E is Young's modulus), the converted equivalent side width of the square cross-section, B = 16.7 mm.

2.4 Constitutive models adopted

The soft clay was modelled by the soft soil model (Neher et al. 2001) and the embankment and the sand layer were modeled by linear elastic model obeying the Mohr- Coulomb failure criterion. The staged construction procedure was used for simulating the embankment loading in 20 different phases and each phase had an embankment height of 0.01 m in centrifuge scale. Coupled consolidation analysis with updated mesh option was used for all phases. The time period for each phase was 30 seconds. The adopted model parameters are listed in Table 1. For soft soil model, the value of the slope of rebound line in e-lnp' plot (e is voids ratio and p' is effective mean stress), κ was assumed as 1/5 of the value of the slope of virgin compression line in e-lnp' plot, λ. The columns were treated as a linear elastic material. The value of poison's ratio (v) was assumed.

The simulated undrained shear strength profile of the soft clay layer is shown in Fig. 4. The model ground had `a thin layer of over consolidated clay underlain by a thick normally consolidated clay. To closely simulate the OCR values of the model ground, the clay layer was divided into three layers with different value of OCR (Fig. 4). The numerical simulation was performed using PLAXIS 3D (2013). The 3D FEA model for the centrifuge test Case 3 is shown in Fig. 5.

Ten-node tetrahedron elements were used to model the whole model. The total number of nodes (vertex plus side nodes) was approximately 104,000 and the total number of elements was about 72,000. The boundary conditions were, at the left and the right (x direction) and the front and the back (y direction) boundaries, the horizontal displacement was fixed but the vertical displacement was allowed. At the bottom boundary both the horizontal and vertical displacements were fixed. Both the ground surface and the bottom boundary (sand layer) were defined as drained, and other boundaries were defined as undrained.

Table 1. Material parameters used in the analysis.

Description	γ (kN/m^3)	λ /(E MN/m^2)	κ/ (v)	c' (kPa)	ϕ' (°)
Embankment	14	(8)	(0.3)	2	30
Clay	13.8	0.213	0.0426	2	25
Sand	18.8	(10)	(0.3)	2	35

Note: γ = unit weight; v = Poisson's ratio; E= elastic modulus; c'= cohesion; ϕ' = friction angle; λ = slope of consolidation line in e-lnp' plot (e is voids ratio and p' is effective mean stress); κ = slope of rebound line in e-lnp' plot

Table 2. Geometrical and engineering properties of model columns (Kitazume and Maruyama, 2007).

Column	Cases	E (MN/m^2)	Dia. (mm)
Acrylic Pipe	Cases 2, 3 and 4	1000	Outer = 19 Inner = 16
Soil-cement columns	Case 7	62.6	20

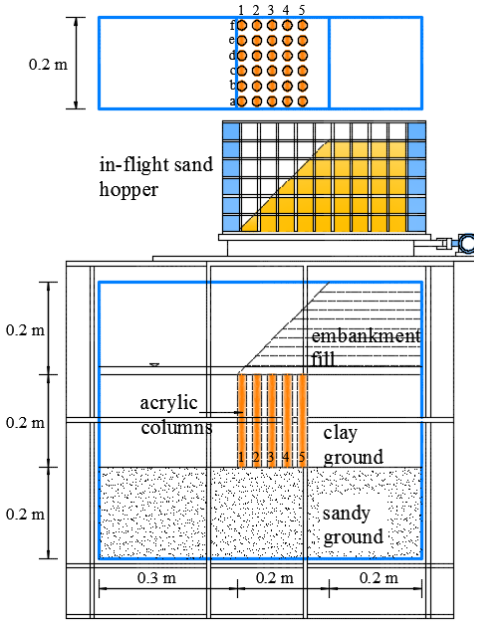

Fig. 3. Model ground setup for Case 3 (modified from Kitazume and Maruyama 2006).

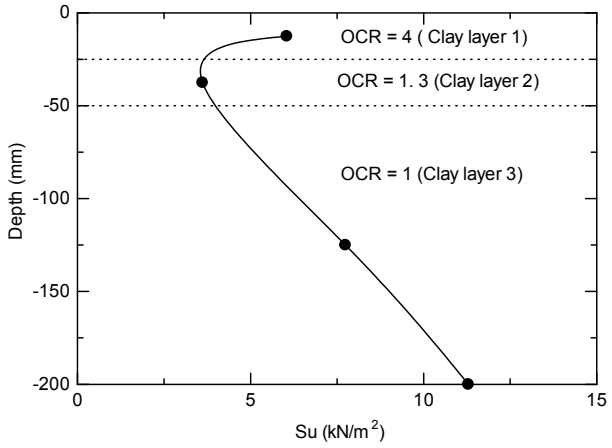

Fig. 4. Simulated undrained shear strength for the soft soil.

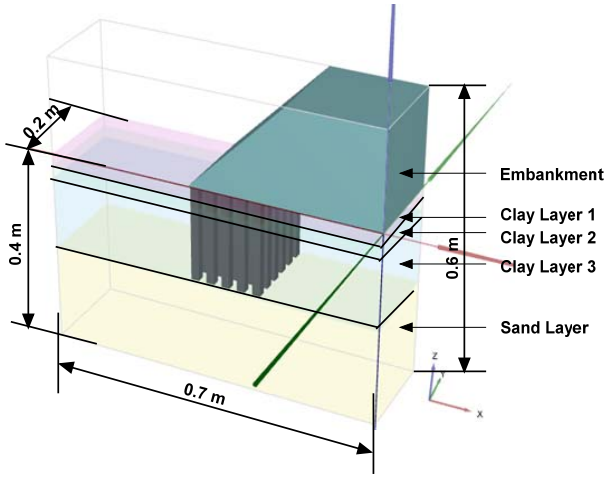

Fig. 5. Case 3/3a 3D model (Centrifuge Model Test).

2.5 Cases investigated

The cases analyzed are listed in Table 3. In the table, Case 3 was simulated with actual model test conditions. While Case 2a, Case 3a, Case 4a were simulated using geometry condition of the model tests, but the modulus of the column adopted was the value of the soil-cement column (but actually it was acrylic pipe). In this way a realistic bending moment and therefore tensile stress in the column can be investigated. Case N1 and Case N2, are assumed for investigating the effect of the improved area (N1) and the length of the column (N2). The plan view of the arrangements of the columns for all cases are shown in Fig. 6.

3. Measured and simulated results

3.1 Case 3

3.1.1 Failure mode of the columns

Figure 7 shows the simulated deformed mesh of Case 3. Kitazume and Maruyama (2007) also observed this kind of deformation mode in the centrifuge model test as shown in Fig. 8. Both the results of FEA and the model test indicate that when the modulus of the column is high, i.e. 1000 MN/m^2, no bending deformation of the columns was observed. All the columns tilted like dominos under the toe of the embankment.

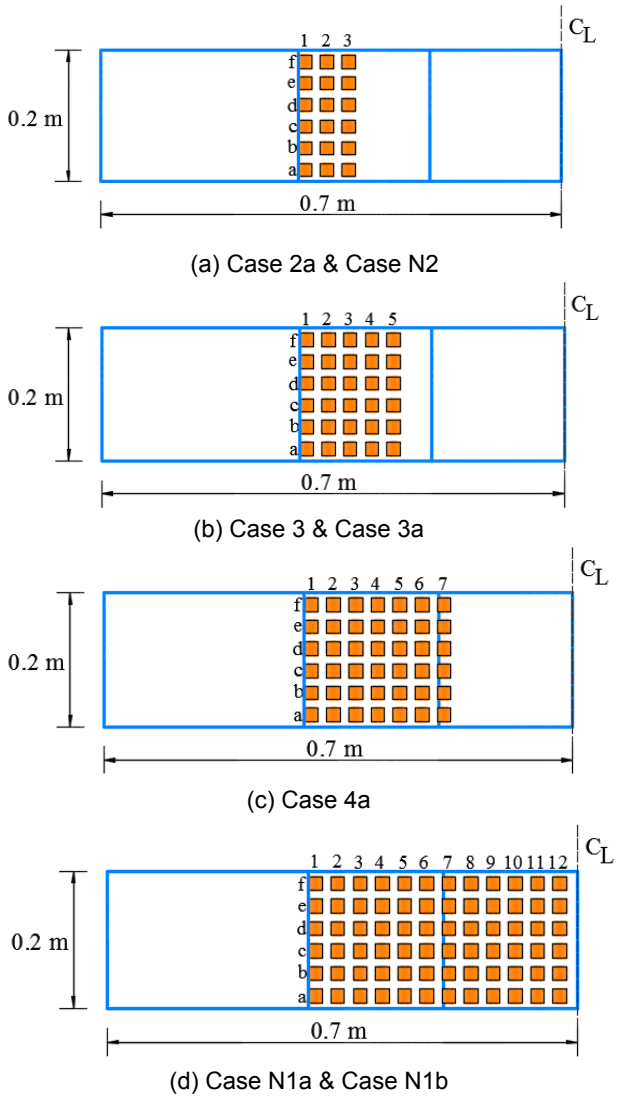

Fig. 6. Plan of the 3D model for different cases.

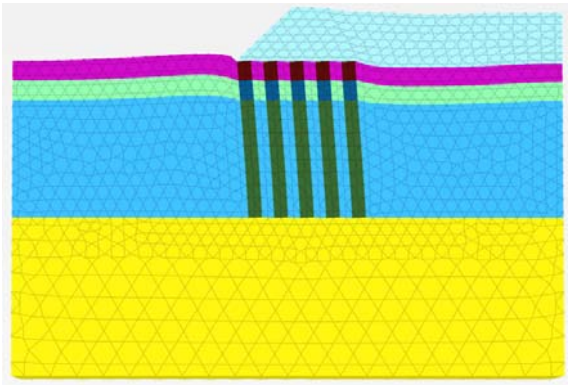

Fig. 7. FEM 3D deformed mesh (Case 3, E=1000 MN/m^2).

Table 3. Cases analyzed.

Case	End bearing or floating	*E* (MN/m^2)	Number of Columns	Length of Columns (m)	Height of embankment (m)
Case 3	End Bearing	1000	5 × 6	10	6
Case 2a	End Bearing	62.6	3 × 6	10	6
Case 3a	End Bearing	62.6	5 × 6	10	6
Case 4a	End Bearing	62.6	7 × 6	10	6
Case N1a	End Bearing	62.6	12 × 6	10	6
Case N1b	End Bearing	62.6	12 × 6	10	4.5
Case N2	Floating	62.6	3 × 6	9.5	4.5

Note: Length of columns and Height of embankment are in prototype scale.

However, when the modulus of the column was reduced to about 62.6 MN/m^2 (Case 3a) as shown in Fig. 9, the simulated results under P_e = 42 kN/m2, clearly show the bending deformation of the columns. P_e is the load under the center of the embankment. Another centrifuge model test Case 7 was conducted with the same number and the arrangement of columns as Case 3, but used soil-cement columns with a diameter of 20 mm. As a reference the measured deformed shapes of the columns of Case 7 are shown in Fig. 10. It can be seen that the deformed shapes of the columns are similar in Figs. 9 and 10.

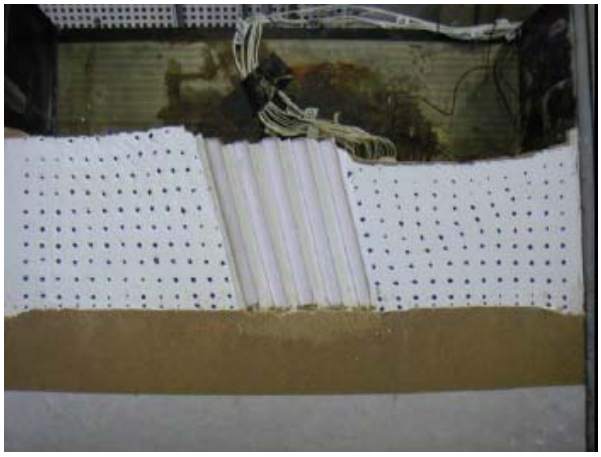

Fig. 8. Column failure for acrylic pipe (Case 3, after Kitazume and Maruyama 2006).

3.1.2 Lateral displacements

For Case 3, comparison of measured and simulated lateral displacement profiles under the toe of the embankment is shown in Fig. 11. It can be seen that at lower embankment load (P_e = 42.2 kN/m^2), the simulated values are smaller than the measured data while at higher embankment load (P_e = 63.8 kN/m^2), the simulation matched the measurement well. The exact reason for the discrepancy under P_e = 42.2 kN/m^2 is not clear yet. It may be due to the soft soil model adopted over-predicted the

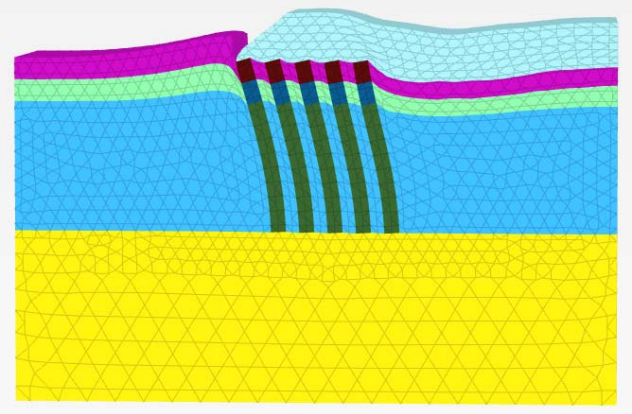

Fig. 9. Case 3a FEM 3D deformed mesh at P_e = 42 kN/m^2 (E=62.6 MN/m^2).

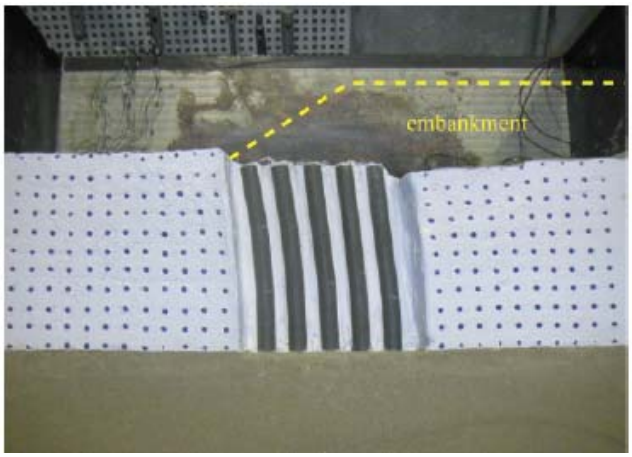

Fig. 10. Measured deformed shapes of column of Case 7 at P_e = 43.9 kN/m^2 (After Kitazume and Maruyama 2007).

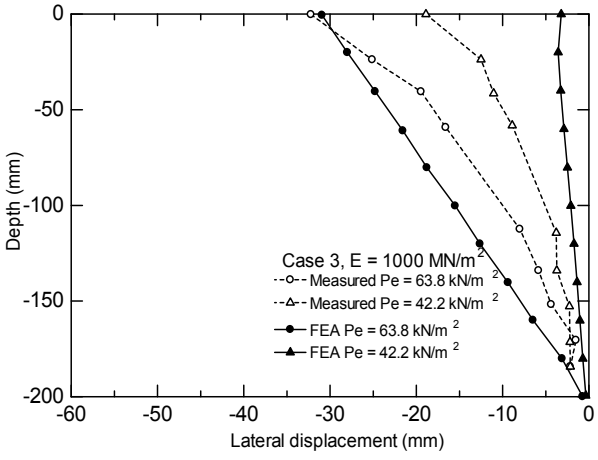

Fig. 11. Lateral displacement profiles (Case 3).

strength of the model ground under plain strain extension condition.

3.1.3 Settlements

The comparison of the measured and simulated settlements for Case 3 is given in Fig. 12. Kitazume and Maruyama (2005) only mentioned that the settlements were measured beside the rearmost column from the toe of the embankment at the side toward the center of the embankment. The simulated settlements are for a point 20 mm away from the edge of the corresponding column. The simulated results underpredicted the settlement in the earlier stage and overpredicted in the latter stage of loading. Although the exact reason is not clear yet, considering no information about precise measurement point, the results are acceptable.

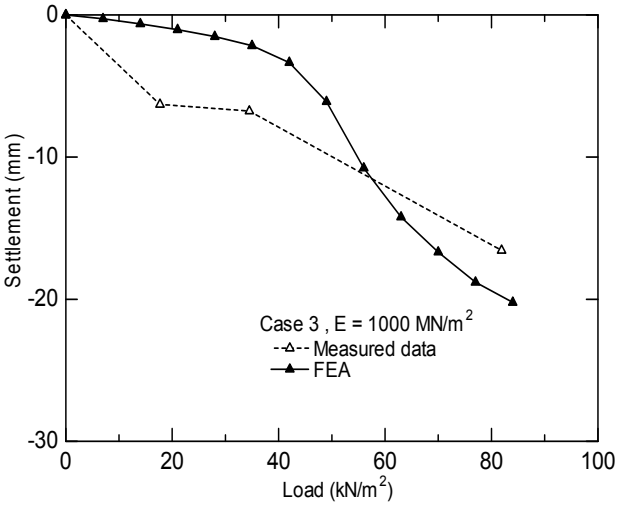

Fig. 12. Settlement profiles.

3.1.4 Bending moments

In 3D FEA, the bending moments in a column were calculated using the stress distributions in the cross-section of the column. The stresses at the edges of the cross-section were obtained by linear extrapolation of the stresses at the integration points of the elements (Chai et al. 2013). The measured and simulated bending moments are compared in Fig. 13. Considering a cross-section with an upward normal, the anti-clockwise moment is defined as positive. The simulated bending moments agree reasonably well with the measurements. An acrylic pipe has a very high strength and no breaking failure took place in the pipe. However, for an ordinary DCM column, the tensile strength of about 100 kN/m^2 can be estimated (1/10 of unconfined compressive strength of about 1,000 kN/m^2) (Igaya et al. 2012). For the model test condition with a bending moment of about 1.03 N•m, the bending induced maximum tensile stress will be about 1332 kN/m^2. This indicates that if using ordinary DCM column, under the same stress conditions, the column will be failed by bending.

In the case only the zone under the toe of the embankment has been improved by the column, the horizontal force from the soft soil of the unimproved zone will be first applied on the columns in the inner row (near the center of the embankment) and the relative larger negative bending moment occurred in upper part of those columns (such as 5d in Fig. 13).

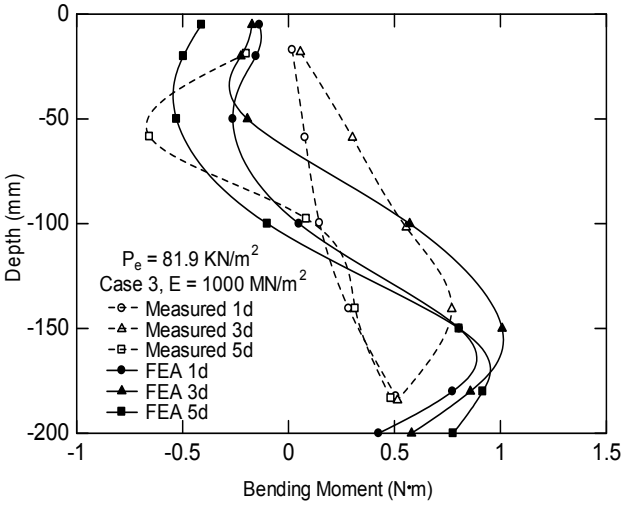

Fig. 13. Bending moment distribution (Case 3).

3.1.5 Discussion

From the above comparison, it can be said that 3D FEA simulated the test results of Case 3 well. The validated numerical procedure will be used to conduct further numerical investigations on the factors affecting bending moment in the column inclusions.

3.2 Numerical investigations

3.2.1 Lateral displacements of columns

(1) Effect of the size of the improved area. Figure 14 shows the influence of the improvement area on the lateral displacement of the column No. 1d (see Fig. 6 for location) under the toe of the embankment. The height of the embankment is 6.0 m (P_e = 84 kN/m^2). For Case 2a with three rows of columns (each row six columns), the maximum lateral displacement is about 52 mm, for Case 3a it is about 50.5 mm, and for Case 4a it is about 48 mm. The lateral displacement reduced with the increase of the improvement area under the toe of the embankment.

(2) Effect of the stiffness of the column. Increasing Young's modulus of the column, *E,* from 62.6 MN/m^2 to 1000 MN/m^2 has an obvious effect on the lateral displacement of the columns as the maximum value reduced from 50.5 mm to 47 mm (Fig. 15). Niu et al. (2006) reported the similar numerical results.

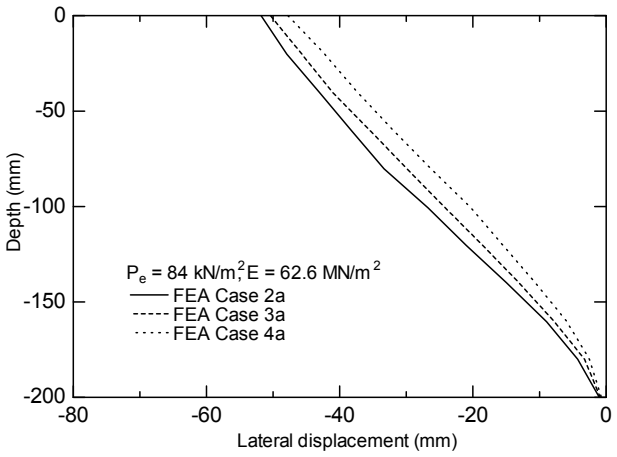

Fig. 14. Effect of improvement rate on lateral displacement.

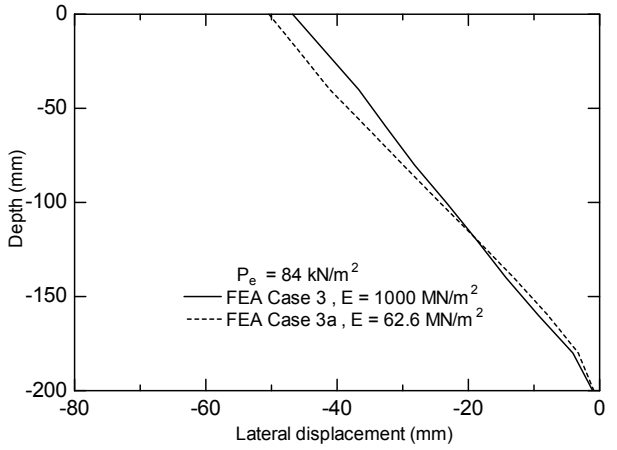

Fig. 15. Effect of stiffness on lateral displacement.

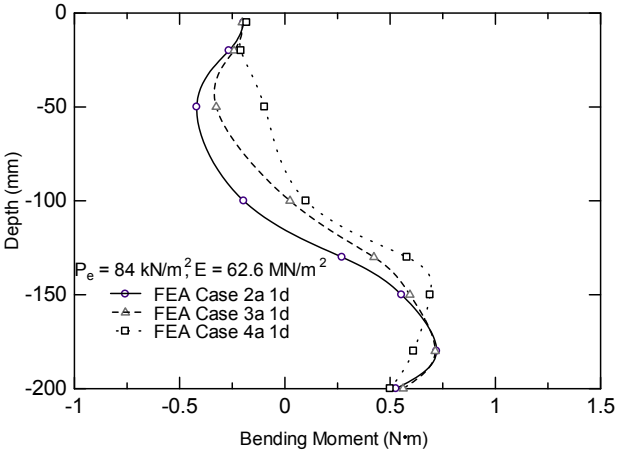

Fig. 16. Effect of improvement rate on bending moment.

3.2.2 Bending moment in the column

(1) Effect of the size of the improved area. Figure 16 shows the simulated bending moments in the column No. 1d of Cases 2a, 3a and 4a. For the bending moment in the upper part of the column, increasing the size of the improvement reduced the absolute maximum bending moment. At the end of the column, the positive bending moment is about the same. The maximum positive bending moment induced tensile stress is about 920 kN/m^2 for the 3 cases, but the absolute negative bending moment induced maximum tensile stresses are 540 kN/m^2, 420 kN/m^2 and 124 kN/m^2 for Case 2a, 3a, 4a, respectively. All of them are larger than 100 kN/m^2 (assumed tensile strength of soil-cement columns) which indicates all the cases will fail by bending failure under a field condition.

(2) Effect of the stiffness of the column. The results of FEA indicate that under the model test condition, for the column with *E* value of 1000 MN/m^2, the maximum moment is about 1.03 N•m and *E* value of 62.6 MN/m^2 of about 0.61 N•m (Fig. 17). Therefore increase the stiffness of the column increases the maximum bending moment. However at the location near the ground surface of the model ground, the absolute value of the negative moment is slightly larger for lower stiffness case.

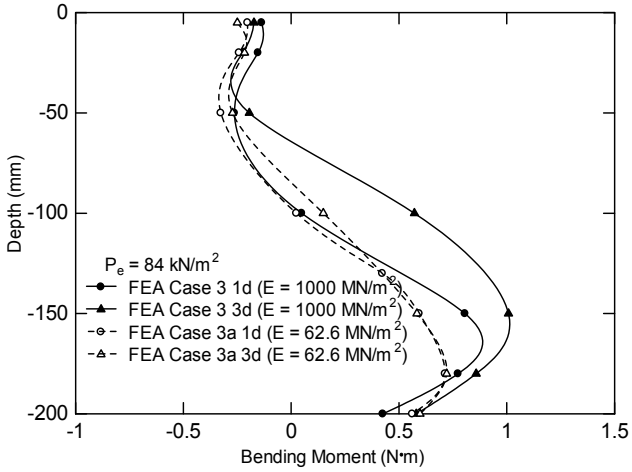

Fig. 17. Effect of stiffness on bending moment.

(3) Embankment height without bending failure. Figure 18 compares bending moment in the column No. 1d and 3d from Case N1a and Case N1b. For the conditions considered reducing the embankment height from 6.0 m (P_e = 84 kN/m^2) to 4.5 m (P_e = 63 kN/m^2) reduced maximum bending moment in the column 1d and 3d significantly. When the height of the embankment is 6.0 m, the bending induced maximum tensile stress is about 252.49 kN/m^2 for 1d and 246 kN/m^2 for 3d while for the height of 4.5 m, the corresponding value is about 48.309 kN/m^2 for 1d and 48.95 kN/m^2 for 3d which is less than 100 kN/m^2 of the assumed tensile strength and the embankment can be safely built under the field condition with a factor of safety for a bending failure of about 2.0. In this case, the load under the center of the embankment is about 13 times of the undrained shear strength of the upper layer of the soft model ground. Further study is needed to propose a design method considering bending

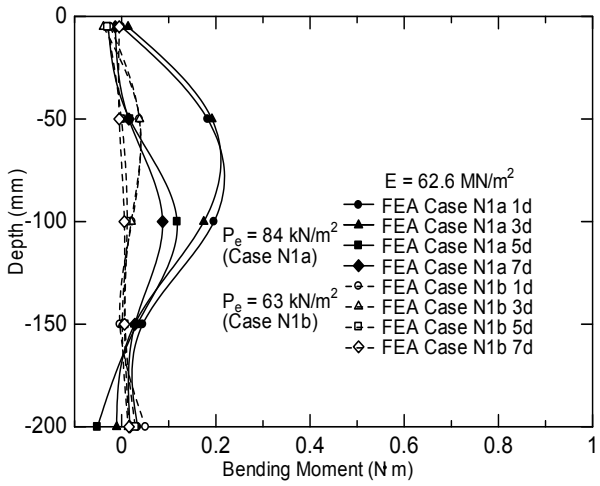

Fig. 18. Effect of embankment loading on bending moment.

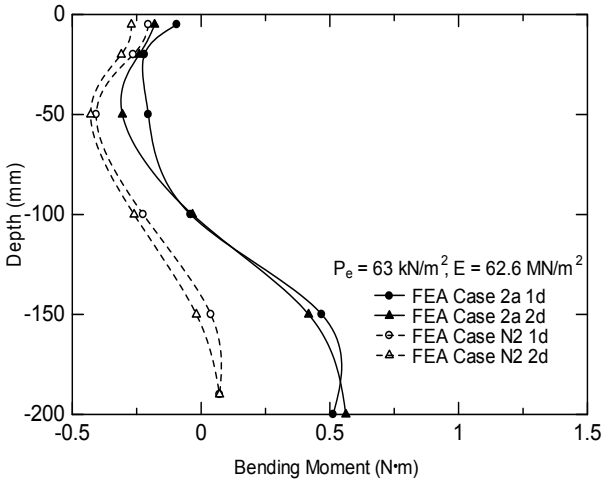

Fig. 19. Bending moment, floating versus end bearing.

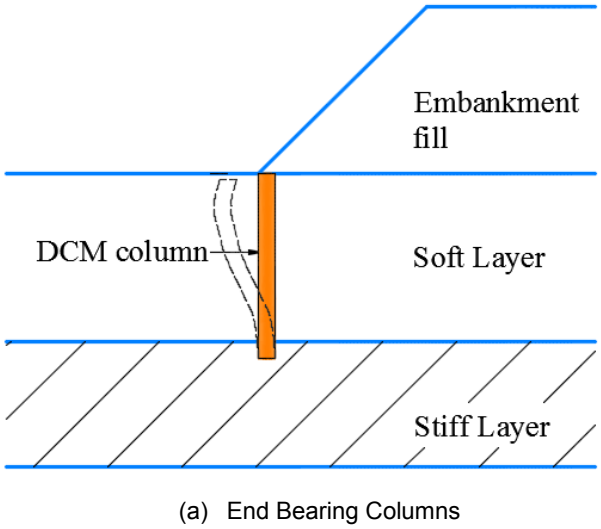

(a) End Bearing Columns

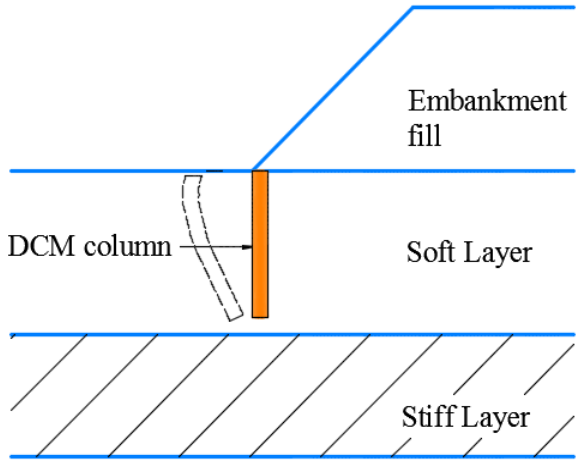

(b) Floating Columns

Fig. 20. Bending shapes.

failure of the column inclusions in the soft deposit under embankment loading.

(4) Floating versus end bearing. For end bearing columns (embedded into stiff sand layer), the simulated maximum bending moment occurs near the end of the column. It is considered that if columns are floated in the soft soil, the moment at the end can be reduced, and also it can reduce the cost of construction. Figure 19 compares the bending moments of the end bearing and floating columns. When the column is floated the bending moment at the end of the column is much smaller than that of the end bearing case. However, the negative bending moment in the upper part of the floated column is higher.

Most natural clayey deposits are just like the model ground considered in this study. There is a stiffer crust at the ground surface, and a weaker layer below it. Considering a column under the toe of an embankment, the deformed column is somehow "S" shaped. Considering a cross-section of the column with its normal upward, the moment will be clockwise (negative) in the upper part and changed to anti-clockwise in the lower part of the column. In case of an end bearing column (Fig. 20a), if the load intensity is high and the lateral displacement of the column is large, the maximum moment will occur in the lower part of the column. While in case of a floating column, most likely the absolute maximum moment will occur in the upper part of the column (Fig. 20b), just as the simulated results in this study.

4. Conclusions

The embankment on DCM column improved soft ground was simulated by three dimensional (3D) finite element analysis (FEA). Firstly one of the centrifuge model tests reported in the literature was simulated by FEA in terms of lateral displacements, settlements and bending moments in the column. The simulated results agreed well with the measured data and the numerical procedure has been verified. Then further numerical investigations were

conducted on factors affecting the bending moment in the column, such as column improved area, stiffness of the column, and the length of the column. Following conclusions can be made from this study.

(1) The simulated results by 3D FEA agreed well with the measured results of a centrifuge model test reported in literature. This indicates that 3D FEA is a powerful tool for investigating the behavior of column inclusions in soft ground under embankment loading.

(2) Regarding to bending moment in the columns, the numerical results show for end bearing columns, increasing the size of the column improvement area, the absolute maximum bending moment was reduced in the upper part of the column, but almost no effect for the moment at the end of the column. Reducing the stiffness of the column, the maximum bending moment in the column was reduced. When the column was “floated” in the soft layer (leaving a thin soft layer without column improvement), the bending moment in the upper part of the column was increased, but the maximum bending moment was reduced.

(3) For end bearing column improvement with an area improvement ratio of 0.28, considering a factor of safety against bending failure of the column of 2.0, the simulated results indicated that an embankment that has a load under the center of the embankment of about 13 times of the initial undrained shear strength of the soft soil can be built.

References

Bergado, D.T., Chai, J.-C., Alfaro, M.C. and Balasubramaniam, A.S., 1994. Improvement techniques of soft ground in subsiding and lowland environment. Balkema, Rotterdam. p. 222.

Broms, B.B., 2004. Lime and lime/cement columns, Ground Improvement, edited by M.P. Moseley and K. Kirsch, Spon Press, Second edition. pp. 252-330.

Chai, J.-C., Liu, S.Y., Du, Y.J., 2002. Field properties and settlement calculation of soil-cement column improved soft subsoil–A case study. Lowland Technology International, **4** (2): 51-58.

Chai, J.-C., Miura, N., Kirekawa, T. and Hino, T., 2009. Settlement prediction for soft ground improved by columns. Proc. Institute of Civil Engineers, Ground Improvement, UK, **163** (2): 109-119.

Chai, J.-C. and Carter, J.P., 2011. Deformation analysis in soft ground improvement. Springer. p. 247.

Chai, J.-C., Shen, S., Ding, W., Zhu, H., & Carter, J., 2013. Numerical Investigation of the failure of a building in Shanghai, China. Computers and Geotechnics, **55**: 482-493.

Chai, J.-C., Shrestha, S., Hino, T., Ding, W.Q., Kamo, Y., and Carter, J., 2015. 2D and 3D analyses of an embankment on clay improved by soil-cement column. Computers and Geotechnics, **68**: 28-37.

Hino, T., Jia, R., Sueyoshi, S. and Harianto, T., 2012. Effect of environment change on the strength of cement/lime treated clays. Front Struct Civil Eng, Higher education Press & Springer, **6** (2): 153-65.

Igaya, Y., Hino, T., and Chai, J.-C., 2012. Laboratory and field strength of cement slurry treated Ariake clay. Proc. 8th International Symposium on Lowland Technology. pp. 40-45.

Kitazume, M. and Maruyama, K., 2005. Collapse failure of group column type deep mixing improved ground under embankment. Pro. International Conf. on Deep Mixing Best Practice and Recent Advances. pp. 245-254.

Kitazume, M. and Maruyama, K., 2006. External Stability of group column type deep mixing improved ground under embankment loading. Soils and Foundations, **46** (3): 323-400.

Kitazume, M. and Maruyama, K. 2007. Internal Stability of group column type deep mixing improved ground under embankment loading. Soils and Foundations, **47** (3): 437-455.

Neher, H. P., Wehnert, M., and Bonnier, P.G., 2001. An evaluation of soft soil models based on trial embankments. Pro. 10th International Conf. on Computer Methods and Advances in Geomechanics, Tucson, Arizona, USA. CRC Press. pp. 373-378.

Niu, J. D., Xu, L. R., Liu, B. C., and Lii, D. W., 2006. 2 D numerical modeling of pile-net composite foundation of high-speed railway embankment in soft soils. In Soft Soil Engineering: Proc. 4th International Conf. on Soft Soil Engineering, Vancouver, Canada. pp. 189-197.

PLAXIS 3D-Version, 2013. PLAXIS Manual, PLAXIS b.v., The Netherlands.

Shen, S-L, Chai, J.-C., and Miura, N., 2001. Stress distribution in composite ground of column-slab system under road pavement. Pro. First Asian-Pacific congress on computational mechanics. Elsevier Science Ltd. pp. 485-490.

Shrestha, S., Chai, J.-C., and Kamo, Y., 2015. 3D numerical simulation of a centrifuge model test of embankment on column improved clayey soil. Proc. 2015 Young Geotechnical Engineers' Symposium on Finite Element Methods, May 17-18, IIT Bombay, Mumbai. Paper No. FEM022.

Yapage, N.N.S., Liyanapathirana, D.S. and Leo, C.J. 2013a. Failure Modes for Geosynthetic Reinforced Column Supported (GRCS) Embankments. Proc. 18th International Conf. Soil Mechanics and Geotechnical Engineering, Paris. pp. 849-852.

Yapage, N.N.S., Liyanapathirana, D.S., Poulos, H.G., Kelly, R.B. and Leo, C.J., 2013b. Analytical Solutions to Evaluate Bending Failure of Column Supported Embankments. IACSIT International J. Engineering and Technology, **5** (4): 502-506.

Zhang, Z., Han, J., and Ye, G., 2014. Numerical analysis of failure modes of deep mixed column-supported embankments on soft soils. Ground Improvement and Geosynthetics, GSP 238, ASCE. pp. 78-87.